RESEARCH PAPER

PCCP
www.rsc.org/pccp

Thermal properties of metastable ices IV and XII: comparison, isotope effects and relative stabilities

Christoph G. Salzmann,* Erwin Mayer and Andreas Hallbrucker

Institute of General, Inorganic and Theoretical Chemistry, University of Innsbruck, A-6020, Innbruck, Austria. E-mail: christoph.salzmann@gmx.at

Received 24th November 2003, Accepted 23rd January 2004
First published as an Advance Article on the web 13th February 2004

Pure samples of H_2O (D_2O) ice IV and of H_2O (D_2O) ice XII were prepared by isobaric heating of high-density amorphous ice at a rate of ≈0.5 K min^{-1} up to ≈175 K and a pressure of 0.81 GPa for ice IV, and at a heating rate of ≈12 K min^{-1} and a pressure of 1.21 GPa for ice XII. The crystalline phases recovered at 77 K and 1 bar were characterized by X-ray diffraction and differential scanning calorimetry (DSC). X-Ray diffractograms of D_2O ice IV show that it transforms directly into cubic ice, and not *via* some amorphous phase as intermediate. The DSC scans of all four types of crystalline phases recorded on heating revealed three thermal features in this order: a reversible endothermic step, an intense exotherm from the phase transition to cubic ice, and a weak exotherm from the cubic → hexagonal ice phase transition. For H_2O (D_2O) ice IV the onset and end temperature of the endothermic step (T_{onset} and T_{end}) are at 139.8 ± 0.3 and 147.1 ± 0.2 K (at 146.2 ± 0.8 and 150.2 ± 0.8 K) on heating at 30 K min^{-1}, and the increase in heat capacity (ΔC_p) is 1.2 ± 0.2 (0.5 ± 0.1) J K^{-1} mol^{-1}. On heating at 5 K min^{-1}, the extrapolated peak onset and peak minimum temperature (T_e and T_{min}) of the phase transition to cubic ice is at 148.7 ± 0.3 and 151.1 ± 0.1 K (at 152.7 ± 0.1 and 155.3 ± 0.2 K), and the enthalpy of the phase transition to cubic ice is −938 ± 14 (−986 ± 14) J mol^{-1}. The corresponding values for H_2O (D_2O) ice XII are for the endothermic step on heating at 30 K min^{-1}: T_{onset} and T_{end} at 131.4 ± 0.8 and 139.5 ± 0.7 K (at 138.1 ± 0.4 and 145.0 ± 0.5 K), and ΔC_p is 1.5 ± 0.2 (1.4 ± 0.2) J K^{-1} mol^{-1}. On heating at 5 K min^{-1}, T_e and T_{min} of the phase transition to cubic ice is at 149.9 ± 0.3 and 153.0 ± 0.2 K (at 154.0 ± 1.2 and 156.9 ± 0.9 K), and the enthalpy of the phase transition to cubic ice is −1233 ± 23 (−1408 ± 8) J mol^{-1}. Therefore, ΔH for the H_2O (D_2O) ice XII to H_2O (D_2O) ice IV phase transition is −295 (−422) J mol^{-1}, and ice XII is more metastable than ice IV at ≈150 K and 1 bar. For H_2O (D_2O) ice XII the endothermic step is separated by a plateau region from the beginning of crystallization, whereas for H_2O (D_2O) ice IV these two thermal effects overlap because its T_{onset} is higher by ≈8 K. T_{onset} and T_e are separated by 4.9 K for D_2O ice IV and 7.3 K for H_2O ice IV. Thus overlap is more pronounced for the former, the endothermic step being cut off by the beginning of crystallization, which is consistent with the lower ΔC_p value for D_2O ice IV. The endothermic DSC features are interpreted as before for H_2O ice XII by Salzmann *et al.* (*Phys. Chem. Chem. Phys.*, 2003, **5**, 3507), in terms of relaxation of the frozen-in proton order–disorder toward equilibrium *via* proton order → disorder transition. When H_2O (D_2O) cubic ice is obtained on heating ice IV, its phase transition to hexagonal ice has a ΔH value of −20 ± 7 (−15 ± 5) J mol^{-1} which is lower than most of the values reported in the literature. We further present new low-frequency Raman spectra of ice XII and show that a peak at 127 cm^{-1} has its counterpart in the Raman spectra of Chou *et al.*'s new "High-Pressure Phase of H_2O Ice" (*Science*, 1998, **281**, 809). This supports our previous conclusion (*J. Phys. Chem. B*, 2002, **106**, 1) that the Chou phase is in fact ice XII. We then conjecture on the solid–liquid phase boundaries of both ice IV and ice XII, and on a metastable triple point where ice IV, ice XII and liquid water are in metastable equilibrium.

Introduction

Ice IV and ice XII are two metastable high-pressure phases of ice. In 1998 Lobban *et al.* first prepared and characterized ice XII by slow crystallization from the liquid phase at 260 K at a pressure of 0.55 GPa.[1] In the same year Chou *et al.* reported a new "High-Pressure Phase of H_2O Ice" in the ice VI domain at 0.7–1.2 GPa and 3–26 °C.[2] They speculated on the relation of their new phase to ice XII but, because of a lack of data, could not confirm it or rule it out. Subsequent to the formation of ice XII from the liquid phase, Koza *et al.* reported the formation of ice XII in a completely different region of the water phase diagram, namely, as an incidental product in the preparation of high-density amorphous ice (HDA) at 77 K on compression of ice I_h up to 1.8 GPa.[3,4] Kohl *et al.* then showed that in this route ice XII forms on compression of ice I_h at 77 K only *via* HDA, and not directly from ice I_h, and that the formation requires a sudden pronounced pressure drop at pressures > 1.1 GPa.[5] They further proposed that shock-wave heating causes transient local heating and crystallization of the ice sample. The structure of ice XII is described by a tetragonal unit cell (space group $I\bar{4}2d$) containing 12 water molecules with four O(1) and eight O(2) oxygen atoms in special positions.[1] The O(2) oxygen atoms are connected by asymmetric H-bonds that form zigzag chains that run along the *a* and *b* axes. These chains are interconnected by O(1)–O(2) H-bonds which results in a structure that "contains only seven- and eight-membered rings and is the first example of a four-connected net of this type".[6]

The existence of ice IV was first suspected in 1912 by Bridgman[7] and later confirmed for D_2O in the pressure range 0.4–0.55 GPa.[8] The difficulty of the ice IV crystallization became

DOI: 10.1039/b315180h

clear in the following when several others failed.[9–11] Evans showed that the formation from the liquid can be induced by appropriate nucleating agents.[12] Engelhardt and Whalley reported that even with the most efficient nucleating agent, "nucleation of ice IV was by no means consistent and only 1 freezing in 10 yielded ice IV".[13] They further stated: "in these experiments, ice IV exists for only a few seconds to several minutes at about −25 °C before transforming spontaneously to a more stable phase". Because of this, ice IV has been called "a will-o′-the-wisp, a tentative, ghostly form of ice".[14] The structure of ice IV was determined by X-ray diffraction[15,16] and its IR spectrum[17] was recorded, using samples that were recovered at 77 K and atmospheric pressure. The structure of ice IV is based on a rhombohedral unit cell (space group $R\bar{3}c$) comprising 16 water molecules with 12 oxygen atoms O(1) in a general position, and 4 oxygen atoms O(2) in a special position.[16] These oxygen atoms are connected through four different asymmetric hydrogen bonds: The first type of O(1)–O(1′) H-bonds assemble a puckered six-ring. A second H-bond of type O(2)–O(2′) passes through the centre of each ring. O(2) atoms are connected with adjacent six-rings through O(1)–O(2″) H-bonds and H-bonds of the type O(1)–O(1‴) connect neighbouring six-rings.

Recently, we showed that the pure ices IV and XII can be formed in a reproducible manner on controlled isobaric heating of HDA at 0.81 GPa up to ∼183 K.[18,19] The essential parameter is the heating rate, slow heating favouring formation of ice IV, whereas faster heating rates lead to formation of ice XII. This approach is complementary to cooling liquid water under pressure and offers a new and reproducible way of preparing ices IV and XII. Raman spectra of recovered ices IV[20] and XII[21] prepared in this manner were recently reported. Comparison of the Raman spectrum of ice XII with that of the new high-pressure phase of H_2O ice reported by Chou *et al.*[2] suggests that their new ice was in fact ice XII.[21]

The structure of ice IV was recently challenged by Henry who calculated a negative hydrogen bonding-energy for ice IV with the PACHA ("partial atomic charges and hardnesses analysis") formalism.[22] Later the structure determined by Engelhardt and Kamb[15,16] was confirmed by neutron diffraction by Klotz *et al.*[23] This shows a recent example of how theoretical models, like PACHA, still fail to predict the properties of supramolecular water-ensembles.

Here we report the thermal properties of recovered ice IV and ice XII for both the H_2O and D_2O phases as studied by differential scanning calorimetry (DSC). The DSC scans of all four types of crystalline phases recorded on heating revealed three thermal features in this order: a reversible endothermic step, an intense exotherm from the phase transition to cubic ice, and a weak exotherm from the cubic → hexagonal ice phase transition. From these data it follows that at ≈150 K and 1 bar, ice XII is more metastable than ice IV. We also present new low-frequency Raman spectra of ice XII and show that a peak at 127 cm^{-1} has its counterpart in the Raman spectra of Chou *et al.*'s new "High-Pressure Phase of H_2O Ice".[2] This supports our previous conclusion that the Chou phase is in fact ice XII.[21] We further conjecture on the solid–liquid phase boundaries of both ice IV and ice XII, and on a metastable triple point where ice IV, ice XII and liquid water are in metastable equilibrium.

We note that the melting line of ice IV and the observed kink on its decompression-induced melting is up to now the most important experimental hint to the existence of a second critical point in the phase diagram of water,[24,25] which is assumed to terminate the equilibrium line between a low-density liquid (LDL) and a high-density liquid (HDL).[26,27] Thus, the properties of ice IV could play a vital role in the liquid–liquid critical point scenario.

Experimental

The procedure of preparing ice IV on isobaric heating of HDA is described in detail in ref. 19. Compared to the pressure vessel used in ref. 19, the pressure vessel used in this study was further improved with a hardened steel plate screwable to the bottom of the piston cylinder apparatus. This allowed the installation of a more effective thermal insulation between the apparatus and the surrounding components of the press, and better control of heating rate. Briefly, 0.500 cm^3 of either D_2O water (from Aldrich, No. 15,188-2, 99.9 atom% D), or of deionized H_2O water, was pipetted into an indium cup in the precooled piston-cylinder apparatus with 9-mm diameter piston. HDA was then made by compression of ice I_h at 77 K up to 1.4 GPa using a computerized "universal testing machine" (Zwick, Model BZ100/TL3S) at a rate of 7000 N min^{-1}. Pressure-displacement curves indicating the phase transition to HDA were recorded with the TestXpert 7.1 software of Zwick and were identical to those reported elsewhere.[5,19,28,29] HDA was then transformed to ice IV on isobaric heating at a rate of ∼0.5 K min^{-1} from 77 to ∼175 K at a pressure of 0.81 GPa.[19] Ice XII samples were crystallized from HDA at 1.21 GPa using a heating rate of ∼12 K min^{-1}. The preparation of ice XII at 1.21 GPa allows the use of a more moderate heating rate compared to 0.81 GPa. A detailed analysis of the crystallization kinetics of HDA as a function of pressure will be reported elsewhere.

The progress of the phase transitions was monitored by temperature-displacement curves. After complete crystallisation, the samples were quenched to 77 K under pressure and then recovered under liquid N_2 after release of pressure. Recovered ice IV and ice XII samples were characterised by X-ray diffraction as shown in Fig. 1.

The X-ray diffractograms were recorded on a diffractometer in θ–θ geometry (Siemens, model D 5000, Cu-Kα), equipped with a low-temperature camera from Paar. Installation of a "Goebel mirror" allowed to record small amounts of sample without distortion of the Bragg peaks. The temperature of the sample plate was controlled by a LakeShore CI330 autotuning temperature controller. Calculation of X-ray diffractograms was performed with the "Powder-Cell" Software (BAM, Bundesanstalt für Materialforschung, Berlin, Germany).

A differential scanning calorimeter (Model DSC-4, Perkin-Elmer) with a self-written computer program was used. After heating each sample from 93 to 253 K and recording its DSC scan, a second heating scan of now ice I_h was recorded and subtracted as a baseline from the initial scan. Between 10.1 and 25.9 mg of sample were transferred under liquid N_2 into steel capsules with screwable lids. The masses of the samples were obtained in a third DSC scan of the endothermic melting of ice I_h, by using the value of 6012 J mol^{-1} (6280 J mol^{-1}) as heat of melting of H_2O (D_2O) ice I_h. The DSC instrument was calibrated with cyclopentane. On heating at 30 K min^{-1} the thermal lag is −1.6 K, and temperatures given in the text are already corrected for this thermal lag. However, temperature scales in the Figures are not corrected. Thermal lag is negligible for heating at 5 or 10 K min^{-1}.

Raman spectra were recorded on a Labram-1B spectrometer equipped with a microscope (from Dilor company), through an ULWD-50 objective (Olympus company), by coadding four sets of spectra with an overall recording time of ≈10 min. A 20 mW He–Ne laser with 632.8 nm wavelength was used, and the 1800 lines mm^{-1} grating provides a resolution of 1.1 cm^{-1} at 150 cm^{-1} increasing to 0.6 cm^{-1} at 3600 cm^{-1}. The abscissa was calibrated with a silicon standard, and the sharp Raman shifts are accurate to ±2 cm^{-1}. An Oxford Microstat was used as cryostat. The temperature of the sample was controlled by a LakeShore CI330 autotuning temperature controller and remained constant within ±0.2 K. Spectra were recorded *in vacuo* at ≈10 mbar.

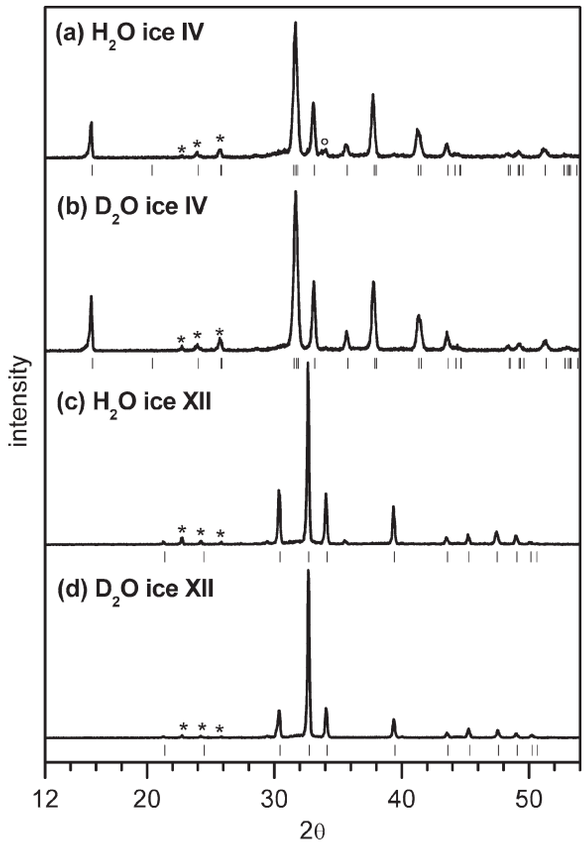

Fig. 1 X-Ray diffractograms (Cu-Kα) of recovered H_2O ice IV (a), D_2O ice IV (b), H_2O ice XII (c) and D_2O ice XII (d), recorded at 90 K. Small peaks marked with asterisks are from ice I_h, the open circle in (a) indicates a minor amount of high-pressure ice impurity. Vertical bars below each diffractogram indicate the peak positions of the simulated diffractograms of the ice phases calculated from the structural data reported in refs. 1, 4, 15, 16 and 23.

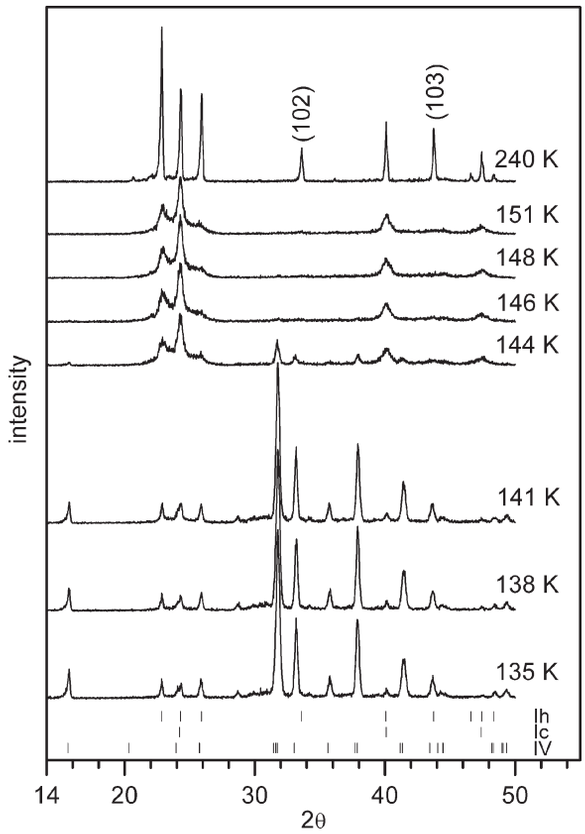

Fig. 2 Conversion of D_2O ice IV to D_2O ice I_c (D_2O ice I_h) as seen in X-ray diffractograms of a sample recorded on heating in steps from 135 to 240 K. The sample was heated from 90 K to increasingly higher temperatures, held at each temperature for 5 min, and cooled to 90 K for recording its diffractogram. Note the absence of broad features attributable to formation of an amorphous water phase. Vertical bars below the diffractograms indicate the peak positions of the simulated diffractograms of ice I_h, ice I_c and ice IV calculated from the structural data.

Results

Fig. 1 shows the X-ray diffractograms of the recovered H_2O ice IV (a), D_2O ice IV (b), H_2O ice XII (c) and D_2O ice XII (d) samples. We made a major effort to obtain the best possible purity of the samples. The diffractograms of the H_2O and D_2O ice XII samples and of the D_2O ice IV sample contained no detectable impurities of other high-pressure phases of ice and thus the purity of those samples is expected to be higher than 99%. The preparation of H_2O ice IV has always been more difficult than D_2O ice IV. This fact has already been outlined by Bridgman[8] and Engelhardt and Whalley[13] in their crystallization experiments of ice IV from the liquid and also in our crystallization experiments of HDA at 0.81 GPa using a heating rate of $\sim$0.5 K min^{-1} and yielding H_2O ice IV samples containing $\sim$6% ice XII.[18,19] This amount could be further reduced, most probably due to the improved thermal insulation of the pressure vessel used in this study. However there is still a small detectable impurity in the diffractogram of H_2O ice IV which is marked by an open circle in Fig. 1(a). The degree of purity of the H_2O ice IV samples is thus expected to be only higher than 97%. The diffractograms contain a minor amount of ice I_h (marked by asterisks) which originates from condensation of water vapour onto the cold sample during the transfer to the precooled X-ray diffraction sample holder. This could be deduced from the absence of a decoupled O–D stretching transition of ice I_h in the Raman spectra of H_2O ice IV or ice XII containing 5% D_2O.[20,21]

In Fig. 2 we show the phase transition of D_2O ice IV to ice I_c followed by X-ray diffraction upon heating *in vacuo*. The sample was heated starting from 90 K to successively higher temperatures. After annealing for 5 min at the temperatures indicated on the right of each diffractogram, the sample was cooled back to 90 K in order to record its diffractogram. There is no change in the diffractograms up to temperatures of 141 K. After annealing at 144 K, a pronounced decrease of the ice IV Bragg peaks is observable and the characteristic reflections of ice I_c appear. This transition is completed after annealing at 146 K. Heating to 240 K leads to formation of ice I_h. The powder pattern of ice I_c can be distinguished from ice I_h through the absence of the hexagonal 102 and 103 reflections. The Bragg peaks of ice I_c show a remarkably larger full width at half maximum than the peaks of ice IV or ice I_h which is attributable to the small crystal size of ice I_c.[30] The appearance of a peak at the low-angle side of the cubic 111 reflection ($2\theta = 24{,}3°$) and a shoulder at the high-angle side are also typical for ice I_c. These features had been attributed by Kuhs *et al.* to stacking faults of the six-membered rings occurring in ice I_c or to hexagonal sequences in the structure.[30]

The diffractograms of ice IV contain a minor amount ($\sim$6%) of ice I_h which originates from condensation of water vapour onto the cold sample and substrate during the transfer (*cf.* above). After conversion of ice IV to ice I_c, this minor amount is not observable anymore. The phase transition to ice I_c is accompanied by a large expansion of volume creating a very loose material. We believe, that the ice I_h that had formed by condensation of water vapour onto the surface of the ice IV is now out of focus of the X-ray beam and that the diffractograms are thus from ice I_c that had crystallized from ice IV.

Fig. 3 depicts the DSC scans of H_2O ice IV (a), D_2O ice IV (b), H_2O ice XII (c) and D_2O ice XII (d) recorded on heating from 93 to 253 K at 5 K min^{-1}. All scans are shown on the same scale and are normalized to 1 mmol which is 18.015 mg for the H_2O polymorphs and 20.023 mg for the D_2O polymorphs. The intense exotherms in all four scans result from the phase transition to ice I_c. The peak minimum of the transition H_2O (D_2O) ice IV to ice I_c is found at 151.1 K (155.4 K) and of the transition H_2O (D_2O) ice XII to ice I_c at 152.9 K (157.6 K). A heating rate of 5 K min^{-1} was found to be optimal to determine the enthalpies for these transitions because at higher heating rates, the exotherms were often accompanied by a strong tailing which made integration ambiguous. Table 1 shows the mean values for the extrapolated onset-temperatures (T_e), the temperatures of peak minima (T_{min}) and the enthalpies of the irreversible transitions to ice I_c (ΔH) including the data from Fig. 3 and three more H_2O and D_2O ice XII and five more H_2O and D_2O ice IV samples.

For the transition of H_2O (D_2O) ice IV to ice I_c ΔH is -938 ± 14 J mol^{-1} (-986 ± 14 J mol^{-1}) which is less exothermic than the transition of H_2O (D_2O) ice XII to ice I_c with a ΔH value of -1233 ± 23 J mol^{-1} (-1408 ± 8 J mol^{-1}). This fact can also be seen at a glance because of the smaller peak heights and areas of the exotherms of the transition of ice IV to ice I_c (Fig. 3(a) and (b)) in comparison with the ice XII to ice I_c exotherms (Fig. 3(c) and (d)). Going from H_2O to D_2O results in a change of -48 ± 28 J mol^{-1} for ice IV, and of -175 ± 31 J mol^{-1} for ice XII. The phase transition of ice XII to ice I_c thus shows a much more pronounced isotope effect than the transition of ice IV to ice I_c.

The ΔH value for the transition H_2O ice XII to ice I_c reported in this study compares well with our previous ones. A value of -1270 ± 50 J mol^{-1} was determined for ice XII containing various amounts of HDA/LDA which had to be taken into account[31] and -1200 ± 70 J mol^{-1} was determined with a heating rate of 10 K min^{-1}.[32] With the use of a 5 K min^{-1} heating rate in this study it was possible to reduce the error range of the ΔH value noticeably.

The temperature T_e (T_{min}) of the exotherm of H_2O ice XII to ice I_c transition is 1.2 ± 0.6 K (1.9 ± 0.2 K) higher than that observed for the ice IV to ice I_c exotherm. A very similar value is found on comparing the D_2O polymorphs: 1.3 ± 1.3 K (1.6 ± 1.1 K). This small shift makes it impossible to resolve two exotherms in DSC scans of ice IV/ice XII mixtures (not shown). Such mixtures can be obtained by heating HDA isobarically at 0.81 GPa with heating rates between $\approx$1 and $\approx$14 K min^{-1}.[18,19] Changing from H_2O ice IV to D_2O ice IV results in an increase of T_e (T_{min}) of 4.0 ± 0.4 K (4.2 ± 0.3 K). Between H_2O ice XII and D_2O ice XII a very similar shift of 4.1 ± 1.5 K (3.9 ± 1.1 K) is observed.

Second and much weaker exothermic transitions in the DSC scans resulting from the phase transitions of ice I_c to ice I_h are found in Fig. 3 at 216 K (a), 219 K (b), 217 K (c) and 222 K (d). Integration of the peaks from Fig. 3 and other experiments gave ΔH values of -20 ± 7 J mol^{-1} (a), -15 ± 5 J mol^{-1} (b), -31 ± 3 J mol^{-1} (c) and -38 ± 8 J mol^{-1} (d). Some of these weak exotherms, especially those from ice I_c obtained from ice IV, were difficult to integrate and were not taken into account. The listed values are thus expected to be upper-bound values. However, it can be seen from the ΔH values and also from the peak heights in Fig. 3, that the phase transition of ice I_c originating from ice XII is more exothermic than that of ice I_c obtained from ice IV.

The third feature in the DSC scans of Fig. 3 is an endothermic step that precedes the intense exotherms. This becomes visible in Fig. 3 only on multiple enlargement (8×). The extrapolated onset-temperatures (T_{onset}) of these endothermic steps on heating at 5 K min^{-1} are found at 135 K (139 K) for H_2O (D_2O) ice IV and at 125 K (131 K) for H_2O (D_2O) ice XII. In the following we used a heating rate of 30 K min^{-1} to make these weak features better observable.

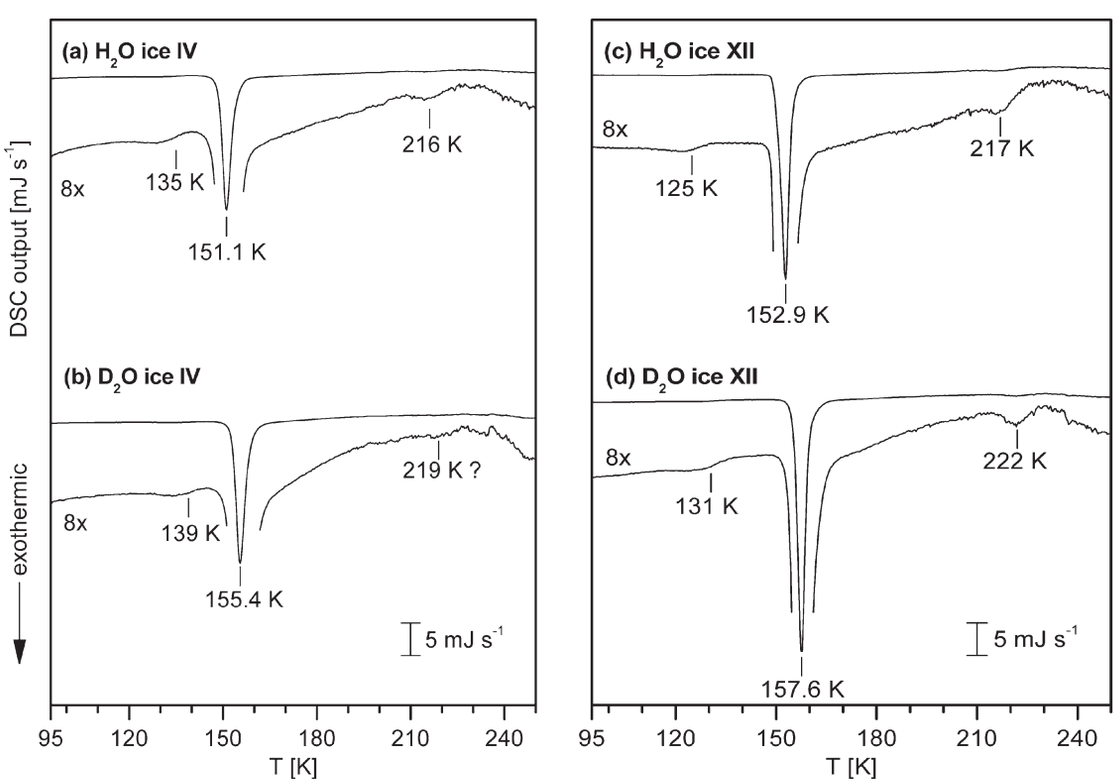

Fig. 3 DSC scans of recovered (left) H_2O ice IV (a), D_2O ice IV (b), (right) H_2O ice XII (c) and D_2O ice XII (d), recorded on heating from 93 to 253 K with 5 K min^{-1}. The scans are shown on the same scale and are normalized to 1 mmol which is 18.015 mg for the H_2O polymorphs and 20.023 mg for the D_2O polymorphs. The four DSC scans are also depicted 8-fold enlarged in order to show the endothermic steps at low temperatures, and the weak exotherms from the ice $I_c \rightarrow$ ice I_h phase transition.

Table 1 Enthalpies ΔH and temperatures of the irreversible transformation of H_2O and D_2O ices IV and XII to ice I_c, followed by DSC with a heating rate of 5 K min^{-1}

Phase of ice	T_e[a] /K	T_{min}[a] /K	ΔH/J mol^{-1}
H_2O ice IV	148.7 ± 0.3	151.1 ± 0.1	-938 ± 14
D_2O ice IV	152.7 ± 0.1	155.3 ± 0.2	-986 ± 14
H_2O ice XII	149.9 ± 0.3	153.0 ± 0.2	-1233 ± 23[b]
D_2O ice XII	154.0 ± 1.2	156.9 ± 0.9	-1408 ± 8

[a] T_e: Extrapolated peak onset temperature; T_{min}: temperature of peak minimum. [b] Compare with refs. 31 and 32.

Fig. 4 shows the DSC scans of H_2O ice IV (1a–1d), D_2O ice IV (2a–2d), H_2O ice XII (3a–3d) and D_2O ice XII (4a–4d) recorded on heating from 93 K at 30 K min^{-1}. Curves (1a)–(4a) were recorded on heating the samples from 93 to 253 K. Scans (b)–(d) demonstrate the reversibility of the endothermic steps. Scans (1b)–(4b) are the scans of new samples recorded on first heating from 93 to 149 K (1b), 152 K (2b), 150 K (3b) and 153 K (4b). After cooling to 93 K at 30 K min^{-1}, the scans of the same samples recorded on second heating to the same temperatures are shown as curves (1c)–(4c). After second cooling to 93 K, the scans recorded on third heating to 253 K are shown as curves (1d)–(4d). The onset and end temperatures (T_{onset} and T_{end}) of the endothermic steps are indicated by vertical lines. Mean values of T_{onset}, T_{end} and the increase in heat capacity (ΔC_p) are given in Table 2. The analysis of the data was performed as described in ref. 33 and is shown exemplarily for scan (3a) by dashed lines. We also determined for heating at 30 K min^{-1} the mean T_e values of H_2O (D_2O) ice IV which are found at 156.4 (160.1 ± 0.6) and for H_2O (D_2O) ice XII at 156.9 ± 0.3 (161.6 ± 0.3). We note that the method for evaluation of T_{onset} used in this study and proposed in ref. 33 is slightly different from that used in our previous study of the low-temperature dynamics of recovered H_2O ice XII[32] (compare Fig. 4, scan (3a) in this study with Fig. 2, scan (b) in ref. 32). Because of this, T_{onset} and ΔC_p values of H_2O ice XII in ref. 32 differ slightly from those reported here.

Discussion

The reversible endothermic step

One of the most surprising aspects of this study, and our previous one on H_2O ice XII and H_2O ice V,[32] is the observation of an endothermic step, or an increase in C_p with raising temperature, followed by a clear plateau region in the DSC scans of unannealed H_2O and D_2O ice XII (*cf.* Figs. 3 and 4), or of an apparent endothermic peak in DSC scans of unannealed H_2O and D_2O ice IV (*cf.* Figs. 3 and 4), prior to crystallization to ice I_c. These features are remarkably similar to those

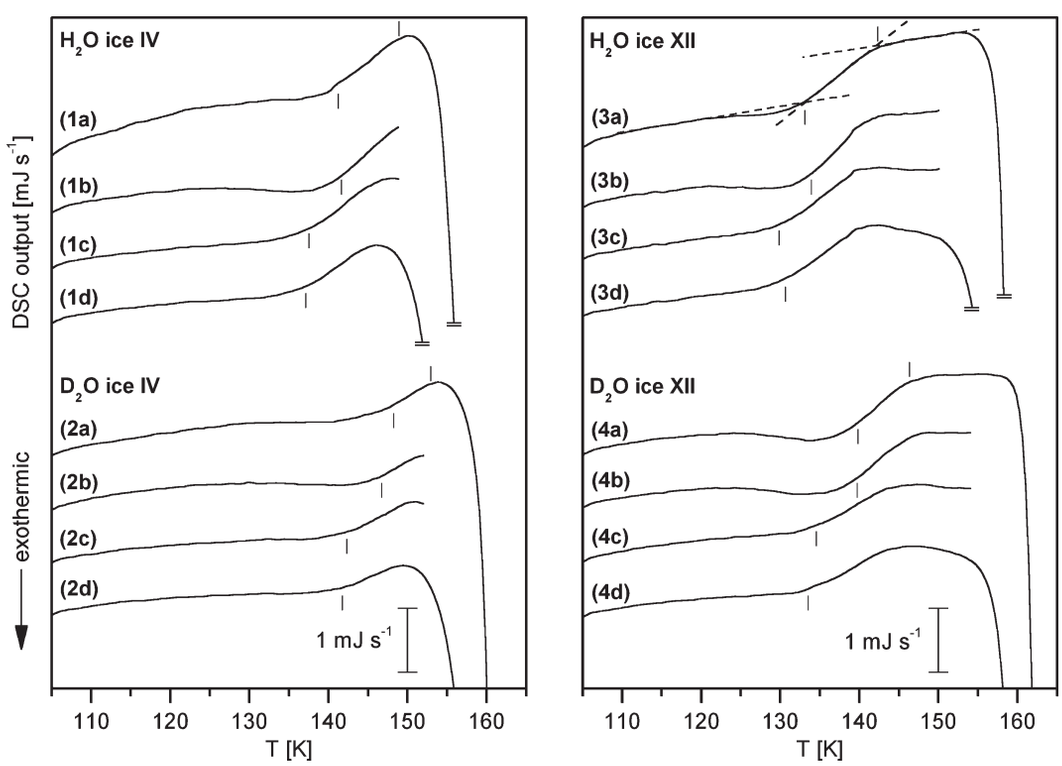

Fig. 4 DSC scans of recovered H_2O ice IV (1a–1d), D_2O ice IV (2a–2d), H_2O ice XII (3a–3d) and D_2O ice XII (4a–4d), recorded on heating at 30 K min^{-1}, starting at 93 K. Curves (1a)–(4a) were recorded on heating the samples from 93 to 253 K. Scans (b)–(d) demonstrate the reversibility of the endothermic steps. Scans (1b)–(4b) are the scans of new samples recorded on first heating from 93 to 149 K (1b), 152 K (2b), 150 K (3b) and 153 K (4b). After cooling to 93 K at 30 K min^{-1}, the scans of the same samples recorded on second heating to the same temperatures are shown as curves (1c)–(4c). After second cooling to 93 K, the scans recorded on third heating to 253 K are shown as curves (1d)–(4d). T_{onset} and T_{end} of the endothermic steps are indicated by vertical lines, and the T_{onset} temperatures corrected for thermal lag are 139.6 K (1a), 140.0 K (1b), 135.9 K (1c), 135.5 K (1d), 146.6 K (2a), 145.1 K (2b), 140.7 K (2c), 140.1 K (2d), 129.5 K (3a), 132.3 K (3b), 128.2 K (3c), 129.0 K (3d), 138.2 K (4a), 138.1 K (4b), 132.9 K (4c) and 131.9 K (4d). T_{end} temperatures are 147.3 K (1a), 151.3 K (2a), 141.7 K (3a) and 145.7 K (4a). The analysis of the data was performed as described in ref. 33 and is shown for scan (3a) by dashed lines. The increase in heat capacity, ΔC_p, is calculated as 1.1 J K^{-1} mol^{-1} (1a), 1.4 J K^{-1} mol^{-1} (1b), 1.6 J K^{-1} mol^{-1} (1c), 1.2 J K^{-1} mol^{-1} (1d), 0.6 J K^{-1} mol^{-1} (2a), 0.6 J K^{-1} mol^{-1} (2b), 0.9 J K^{-1} mol^{-1} (2c), 0.7 J K^{-1} mol^{-1} (2d), 1.5 J K^{-1} mol^{-1} (3a), 1.7 J K^{-1} mol^{-1} (3b), 1.7 J K^{-1} mol^{-1} (3c), 1.7 J K^{-1} mol^{-1} (3d), 1.4 J K^{-1} mol^{-1} (4a), 1.4 J K^{-1} mol^{-1} (4b), 1.3 J K^{-1} mol^{-1} (4c), 1.4 J K^{-1} mol^{-1} (4d). The scans are shown on the same scale and are normalized to 1 mmol, and they are shifted vertically for clarity.

Table 2 ΔC_p values and characteristic temperatures of the reversible endothermic step of H_2O and D_2O ices IV and XII prior to the crystallization to ice I_c, followed by DSC with a heating rate of 30 K min^{-1}

Phase of ice	T_{onset}[a] /K	T_{end}[a] /K	ΔC_p[a] /J mol^{-1} K^{-1}
H_2O ice IV	139.8 ± 0.3	147.1 ± 0.2	1.2 ± 0.2
D_2O ice IV	146.2 ± 0.8	150.2 ± 0.8	0.5 ± 0.1
H_2O ice XII	131.4 ± 0.8	139.5 ± 0.7	1.5 ± 0.2[b]
D_2O ice XII	138.1 ± 0.4	145.0 ± 0.5	1.4 ± 0.2

[a] T_{onset}: Extrapolated onset temperature; T_{end}: extrapolated temperature at end of endothermic step; ΔC_p: increase in heat capacity. The temperatures are corrected for thermal lag of the DSC instrument. [b] Compare with refs. 31 and 32.

observed in DSC scans of glasses in their glass → liquid transition region, but the underlying mechanisms differ.[32,34,35] Refs. 34 and 35 should be consulted for a detailed discussion. A further feature seen in the DSC scans on first heating is an undershoot (*cf.* Fig. 4, curves (1a)–(4a)). An undershoot can arise when the rate of cooling is much greater than the heating rate.[36] This is the case here for samples cooled after their preparation with liquid nitrogen.

The most apparent difference between the DSC scans of ice IV and ice XII at low temperatures, prior to crystallization to ice I_c, is that in case of ice XII (Fig. 4, scans (3a) and (4a)) the endothermic step and the beginning of crystallization to ice I_c are clearly separated by a plateau region whereas in case of ice IV (Fig. 4, scans (1a) and (2a)) the endothermic step and the beginning of crystallization seem to overlap. For a heating rate of 5 K min^{-1}, the T_e values of the crystallization of H_2O (D_2O) ice IV and H_2O (D_2O) ice XII differ by only about 1 K, with ice IV showing the lower temperature values (*cf.* Fig. 3 and Table 1). At a heating rate of 30 K min^{-1}, the mean T_e values of H_2O (D_2O) ice IV are found at 156.4 (160.1 ± 0.6), and for H_2O (D_2O) ice XII at 156.9 ± 0.3 (161.6 ± 0.3). The difference of ~1 K persists also for a heating rate of 30 K min^{-1}. A much larger difference is found for T_{onset} of the endothermic step between H_2O (D_2O) ice IV and H_2O (D_2O) ice XII (*cf.* Table 2): 8.4 ± 1.0 K (8.1 ± 1.2 K). Thus, T_{onset} of the endothermic step of ice IV is about 8 K higher than T_{onset} of ice XII whereas the crystallization starts at about a 1 K lower temperature. Summarizing these values it becomes clear why the endothermic step and the beginning of crystallization overlap much more in the scans of ice IV than in those of ice XII. Because of this the endotherm in ice IV samples is partially masked by the intense exotherm.

Furthermore, the temperature interval between T_{onset} and T_e (the beginning of crystallization) is larger for H_2O ice IV than for D_2O ice IV (16.6 *vs.* 13.9 K). This explains why ΔC_p of H_2O ice IV is larger than that of D_2O ice IV (*cf.* Table 2) because for the latter a larger part of the endotherm is concealed by the exotherm.

We recently reported a DSC study of the low-temperature dynamics of recovered H_2O ice XII, and its comparison with that of recovered H_2O ice V.[32] Reversible endothermic steps in DSC scans in unannealed samples of ice V and ice XII were attributed to kinetic unfreezing of proton order–disorder on heating, relaxation toward the equilibrium being attained *via* a proton order → disorder transition. We interpret the reversible endothermic steps observed in the DSC scans of H_2O (D_2O) ice IV and ice XII in the same manner, and ref. 32 should be consulted for further details of the argumentation in this assignment.

In H_2O (D_2O) ice IV T_{onset} of the endothermic step is ≈8 K higher than in H_2O (D_2O) ice XII (*cf.* Fig. 4 and Table 2). This means that at a given temperature the orientational relaxation time of ice IV is slower than that of ice XII.

The irreversible phase transition to cubic ice

We have studied recently the phase transition of recovered H_2O ice XII to ice I_c at 1 bar by X-ray diffraction, Raman spectroscopy, and DSC measurements.[21,31,32] These studies showed that ice XII transforms directly into ice I_c, and not *via* some amorphous phase, and they are in conflict with a recent report of the Raman spectrum of ice XII and of "formation of amorphous ice on careful annealing of ice XII".[37] However, in the latter study the Raman spectra differed strongly from those of ice XII presented in ref. 21, and the structure of ice XII used in that study was not confirmed by diffraction.

In the same manner we investigated whether ice IV transforms directly into ice I_c, or *via* some amorphous phase as intermediate. In Fig. 2 the diffractogram recorded after annealing at 144 K shows the simultaneous existence of ice IV and ice I_c and thus ice IV transforms directly into ice I_c, like the high-pressure phases of ice II, IX, V, VI and XII and not *via* some amorphous phase.[31,38–42] If ice IV were to transform first into an amorphous phase and then into ice I_c, the conversion of the amorphous phase into ice I_c would have to be very rapid to become unobservable in our measurements. Thus, formation of an amorphous phase on heating of ice VIII, before the transition to ice I_c, seems to be the only case showing this behaviour.[43]

The phase transition of ice XII to ice I_c shows a much more pronounced isotope effect than the transition of ice IV to ice I_c. Going from H_2O to D_2O results for ice IV in a change of -48 ± 28 J mol^{-1}, and for ice XII of -175 ± 31 J mol^{-1} (calculated from values in Table 1). To our knowledge only the H_2O forms of the other high-pressure phases of ice and their transition to ice I_c had been studied by calorimetry, and their D_2O isotope effect is not known. We therefore refrain from speculations on the large isotope effect observed for the ice XII → ice I_c transition until data from other high-pressure forms of ice allow a comparison.

The phase transition of H_2O ice I_c to H_2O ice I_h

Heating of ice IV at atmospheric pressure represents a new preparation method for ice I_c. The properties of ice I_c (*e.g.* enthalpy of transition to ice I_h[40,44] and high-resolution neutron diffraction features[30,45]) depend strongly on from which high-pressure phase of ice it is crystallized and so the properties of ice I_c formed on heating ice IV or ice XII may now be compared with previous data. The enthalpies of the transition to ice I_h determined in this study are -20 ± 7 J mol^{-1} for ice I_c with origin ice IV and -31 ± 3 J mol^{-1} for ice I_c which originates from ice XII.

Other ΔH values of the ice I_c → ice I_h transition were reported by Handa *et al.* for ice I_c with origins from ice II (-36.2 ± 4 J mol^{-1}), ice IX (-13.2 ± 4 J mol^{-1}), ice V(-50.7 ± 1 J mol^{-1}), ice VI (-50.2 ± 3 J mol^{-1}), ice VIII (-34.5 ± 3 J mol^{-1}), and low-density amorphous ice (-35 ± 3 J mol^{-1}).[40,44] According to Handa *et al.*, the possible causes for these different values are "the formation of ice I_c with a substantial fraction of stacking faults, the formation of regular stacking variants that are intermediate between ice I_h and I_c, and transformation of ice I_c to I_h that releases some of its heat too slowly to detect, and formation of ice I_c having grains that are small enough to have an energy of some tens of joules per mole".[44] The structure of ice I_c with different origins was analysed with neutron diffraction by Arnold *et al.*:[45] For ice I_c with origin ice IX they reported a pronounced peak on the low-angle side of the cubic 111 reflection. For ice I_c with origin ice II or ice V, this feature was only visible as a shoulder. The ΔH values for the transition of ice I_c (origin ice II or ice V) to ice I_h are among the most exothermic values reported so far, whereas the transition of

ice I_c (origin ice IX) shows the lowest reported value. From the X-ray diffractograms of ice I_c reported in this study (*cf.* Fig. 2) and ref. 31, we calculated the ratio of the heights of the peak on the low-angle side and the cubic 111 reflection for ice I_c with origin ice IV (0.48) and ice XII (0.40). The peak on the low-angle side of the 111 reflection of ice I_c is thus more pronounced for ice I_c with origin ice IV compared to ice I_c which originates from ice XII. This goes along with the less exothermic ΔH value of the transition ice I_c (origin ice IV) $\rightarrow$ ice I_h. These findings seem to support the fact that a more pronounced peak on the low-angle side of the cubic 111 reflection corresponds to a less exothermic enthalpy for the transition ice $I_c \rightarrow$ ice I_h.

According to Kuhs *et al.*, the presence of the non-cubic Bragg peak on the low-angle side of the cubic 111 reflection, which can be indexed as 100 in the lattice of ice I_h, is explainable in terms of hexagonal sequences in the stacking.[30] An increased amount of hexagonal sequences in the ice I_c structure seems thus to correlate with a less exothermic transition of ice I_c to ice I_h.

The ice XII $\leftrightarrow$ ice IV transition, the liquidus lines for metastable ices IV and XII, and the metastable ice IV–ice XII–liquid water triple point

From the ΔH values of the phase transition to cubic ice listed in Table 1 the ΔH values for ice XII $\rightarrow$ ice IV can be calculated: at $\approx$150 K, ΔH for the H_2O (D_2O) ice XII to H_2O (D_2O) ice IV phase transition is -295 (-422) J mol^{-1}. In this temperature range both phases are expected to be nearly fully disordered and the difference in entropy (ΔS) between the two phases is expected to be small. Therefore, ice XII is more metastable (less stable) than ice IV at $\approx$150 K and 1 bar. This is consistent with Klotz *et al.*'s[23] *in-situ* neutron diffraction study of D_2O HDA and its crystallization where D_2O ice XII was observed to transform to D_2O ice IV between 0.6–0.7 GPa and 200–210 K (*cf.* Fig. 3 in ref. 23).

We recently proposed that the new "high-pressure phase of H_2O ice" reported by Chou *et al.*[2] is in fact ice XII.[21] The evidence was the comparison of the Raman spectrum of H_2O ice XII recorded at 130 K *in vacuo*, with that of a new "high-pressure phase of H_2O ice" recorded by Chou *et al.*[2] at 243 K and 0.7–1.2 GPa, and Fig. 4 in ref. 21 shows this comparison. The correspondence between the two Raman spectra in the low-frequency region was taken as a strong support that the new high-pressure phase is in fact ice XII. Since then improved alignment of our Raman spectrometer and use of a new Notch filter enabled us to record spectra to lower frequency, and to observe a further weak Raman band of ice XII. This ice XII spectrum is shown here in Fig. 5 and it is compared with that reported by Chou *et al.*[2] Agreement between the two Raman spectra in the characteristic translational region is remarkable and the differences of both to the low-frequency spectra of the other polymorphs of ice are conspicuous (*cf.* Fig. 4 in ref. 2 and Fig. 7 in ref. 46). Raman bands of ice XII centered at 195 and 127 cm^{-1} have counterparts in the spectrum of Chou *et al.* at 192 and $\approx$123 cm^{-1} (read from Fig. 4 in ref. 2). Shoulders on the high- and low-frequency side of the band centered at 195 cm^{-1} at $\approx$250 and $\approx$158 cm^{-1} can also be detected weakly in the Raman spectrum of the Chou phase (marked by vertical lines). We note that the weak Raman band at $\approx$123 cm^{-1} in the new ice phase is expected to be real because bands of similar, weak, intensity and at similar frequency in the Raman spectra of ice V (*cf.* Fig. 4 in ref. 2) are accepted in the literature as Raman bands (*cf.* Figs. 7 and 8 in ref. 46). We thus conclude that the observation of a further low-frequency band in the Raman spectrum of ice XII and its correspondence with one reported for the new ice phase strongly supports our previous conclusion that this new ice phase is in fact ice XII.

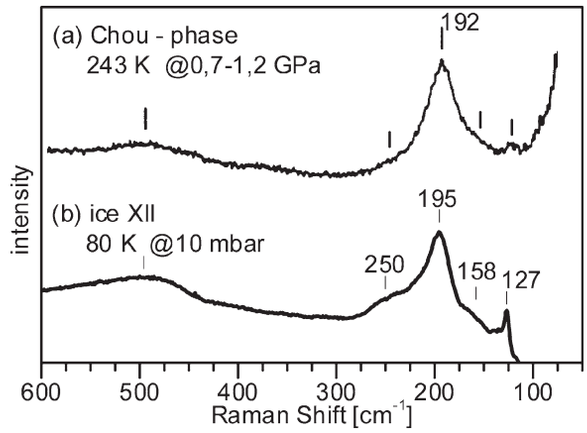

Fig. 5 Comparison of the Raman spectrum of H_2O ice XII recorded *in vacuo* at 80 K from 600 to 100 cm^{-1}, with that of a new "high-pressure phase of H_2O ice" reported by Chou *et al.*[2] Note the new weak Raman band at 127 cm^{-1} in the ice XII spectrum,[21] and its counterpart in the spectrum of the Chou-phase at $\approx$123 cm^{-1}.

Our Raman spectra of ice XII and the spectra of the Chou phase[2] were recorded at clearly different p/T conditions. The temperature and pressure dependences of peak positions can be estimated with the use of the already reported $(d\nu/dT)_p$ and $(d\nu/dp)_T$ values of the various polymorphs of ice.[20,21,46,47] For the low-frequency translation modes, $(d\nu/dT)_p$ values are reported to show a negative algebraic sign, whereas the $(d\nu/dp)_T$ values exhibit a positive sign. Increasing pressure and increasing temperature have thus a compensating effect on the positions of the peaks. This explains qualitatively the quite similar peak positions in our Raman spectra of ice XII (recorded at 80 K and 1 bar) and in the spectra reported by Chou *et al.* (recorded at 0.7–1.2 GPa and 243 K, ref. 2).

In Fig. 6 we compare the melting line of ice IV (squares, data points from ref. 48) with that of the new "high-pressure phase of H_2O ice" (triangles, data points from ref. 2) attributed above to ice XII. The two melting lines have different gradients and must cross eventually. On extrapolating the ice XII melting line (indicated by the broken line) this is expected to happen at $\approx$0.5–0.6 GPa and $\approx$267 K. Thus, at these p/T conditions ice IV, ice XII and liquid water are expected to coexist in metastable equilibrium, which is represented by a new metastable triple point. According to neutron diffraction studies the ice XII and ice IV phases are fully hydrogen disordered.[1,23] Between two disordered phases ΔS is almost

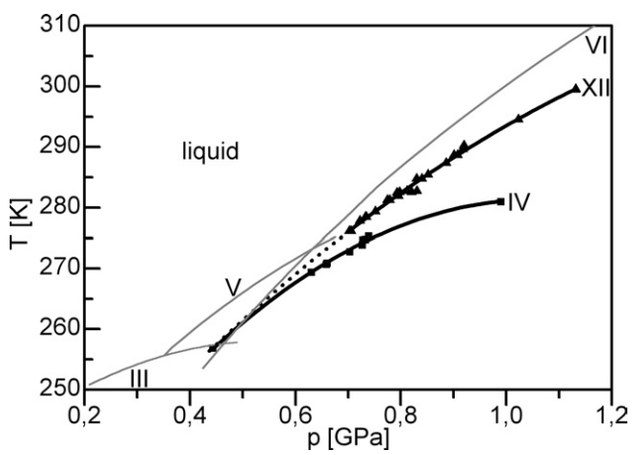

Fig. 6 The relevant part of the phase diagram of water containing the melting lines of ice IV (squares)[48] and the new "high-pressure phase of H_2O ice" reported by Chou *et al.* (triangles)[2] drawn as black lines and the melting lines of ice VI,[2,13] ice V,[13] and ice III[13] represented by thinner grey lines.

zero.[49] Therefore, the phase boundary between ice IV and ice XII is approximately parallel to the temperature axis.

Since in Fig. 6 the melting line of ice IV is above that of ice XII *below* a pressure of ≈0.5–0.6 GPa, ice IV is relatively more stable than ice XII and consequently ice XII should transform into ice IV. This type of conversion had been observed by Klotz *et al.*,[23] D_2O ice XII transforming into D_2O ice IV between 0.6–0.7 GPa and 200–210 K. We note that in their study the accuracy of their pressure values is estimated as ≈0.1 GPa, and thus their pressure is within the range expected for the ice XII → ice IV transition. At pressures *above* ≈0.5–0.6 GPa the melting line of ice XII is above that of ice IV, and thus, ice IV is expected to transform into the relatively more stable ice XII.

That ice IV must transform at high pressures to ice XII, is also consistent with the differences of their densities. The density of ice IV is 1.27 g cm^{-3},[13] and that of ice XII is 1.30 g cm^{-3} (ref. 3) for both at 1 bar and 110 and 127 K, respectively. This difference in densities persists at high pressures, ice IV always being slightly less dense than ice XII.[1,23] Because of the difference in densities, the denser phase ice XII becomes at high pressures less metastable (relatively more stable) than the ice IV phase. The pressure, where the Gibbs energy between ice IV and ice XII becomes zero can be calculated as shown in refs. 50 and 51. We refrain from giving that calculation because we found that even small changes in densities have a large effect.

Acknowledgements

We are grateful for financial support to the ''Forschungsförderungsfonds'' of Austria (project No. P13930-PHY) and to the University of Innsbruck.

References

1 C. Lobban, J. L. Finney and W. F. Kuhs, *Nature*, 1998, **391**, 268.
2 I.-M. Chou, J. G. Blank, A. F. Goncharov, H.-K. Mao and R. J. Hemley, *Science*, 1998, **281**, 809.
3 M. Koza, H. Schober, A. Tölle, F. Fujara and T. Hansen, *Nature*, 1999, **397**, 660.
4 M. M. Koza, H. Schober, T. Hansen, A. Tölle and F. Fujara, *Phys. Rev. Lett.*, 2000, **84**, 4112.
5 I. Kohl, E. Mayer and A. Hallbrucker, *Phys. Chem. Chem. Phys.*, 2001, **3**, 602.
6 M. O'Keeffe, *Nature*, 1998, **392**, 879.
7 P. W. Bridgman, *Proc. Am. Acad. Arts Sci.*, 1912, **47**, 441.
8 P. W. Bridgman, *J. Chem. Phys.*, 1935, **3**, 597.
9 G. J. Wilson, R. K. Chan, D. W. Davidson and E. Whalley, *J. Chem. Phys.*, 1965, **43**, 2384.
10 B. Kamb, A. Prakash and C. Knobler, *Acta Crystallogr.*, 1967, **22**, 706.
11 J. P. Marckmann and E. Whalley, *J. Chem. Phys.*, 1964, **41**, 1450.
12 L. F. Evans, *J. Appl. Phys.*, 1967, **38**, 4930.
13 H. Engelhardt and E. Whalley, *J. Chem. Phys.*, 1972, **56**, 2678.
14 P. Ball, *H_2O A Biography of Water*, Weidenfeld & Nicolson, 1999.
15 H. Engelhard and B. Kamb, *J. Glaciol.*, 1978, **21**, 51.
16 H. Engelhardt and B. Kamb, *J. Chem. Phys.*, 1981, **75**, 5887.
17 H. Engelhardt and E. Whalley, *J. Chem. Phys.*, 1979, **71**, 4050.
18 C. G. Salzmann, T. Loerting, I. Kohl, E. Mayer and A. Hallbrucker, *Can. J. Phys.*, 2003, **81**, 25.
19 C. G. Salzmann, T. Loerting, I. Kohl, E. Mayer and A. Hallbrucker, *J. Phys. Chem. B*, 2002, **106**, 5587.
20 C. G. Salzmann, I. Kohl, T. Loerting, E. Mayer and A. Hallbrucker, *J. Phys. Chem. B*, 2003, **107**, 2802.
21 C. Salzmann, I. Kohl, T. Loerting, E. Mayer and A. Hallbrucker, *J. Phys. Chem. B*, 2002, **106**, 1.
22 M. Henry, *Chem. Phys. Chem.*, 2002, **3**, 607.
23 S. Klotz, G. Hamel, J. S. Loveday, R. J. Nelmes and M. Guthrie, *Z. Kristallogr.*, 2003, **218**, 117.
24 O. Mishima and H. E. Stanley, *Nature*, 1998, **392**, 164.
25 O. Mishima, *Phys. Rev. Lett.*, 2000, **85**, 334.
26 P. G. Debenedetti, *Nature*, 1998, **392**, 127.
27 P. G. Debenedetti and H. E. Stanley, *Phys. Today*, 2003, 40.
28 O. Mishima, L. D. Calvert and E. Whalley, *Nature*, 1984, **310**, 393.
29 O. Mishima, L. D. Calvert and E. Whalley, *Nature*, 1985, **314**, 76.
30 W. F. Kuhs, D. V. Bliss and J. L. Finney, *J. Phys. Colloq., C1*, 1987, **48**, 631.
31 I. Kohl, E. Mayer and A. Hallbrucker, *J. Phys. Chem. B*, 2000, **104**, 12 102.
32 C. G. Salzmann, I. Kohl, T. Loerting, E. Mayer and A. Hallbrucker, *Phys. Chem. Chem. Phys.*, 2003, **5**, 3507.
33 G. Höhne, W. Hemminger and H.-J. Flammersheim, *Differential Scanning Calorimetry – An Introduction for Practitioners*, Springer, Berlin, 1996.
34 G. P. Johari, *Chem. Phys.*, 2000, **258**, 277.
35 G. P. Johari, *J. Chem. Phys. B*, 2003, **107**, 9063.
36 G. W. Scherer, *Relaxation in Glass and Composites*, John Wiley & Sons, New York, 1986.
37 C. A. Tulk and D. D. Klug, *Phys. Rev. B*, 2001, **63**, 212 201.
38 J. E. Bertie, L. D. Calvert and E. Whalley, *Can. J. Chem.*, 1963, **38**, 840.
39 J. E. Bertie, L. D. Calvert and E. Whalley, *Can. J. Chem.*, 1964, **42**, 1373.
40 Y. P. Handa, D. D. Klug and E. Whalley, *J. Chem. Phys.*, 1986, **84**, 7009.
41 Y. P. Handa, D. D. Klug and E. Whalley, *J. Phys.*, 1987, **C1**, 435.
42 Y. P. Handa, O. Mishima and E. Whalley, *J. Chem. Phys.*, 1986, **84**, 2766.
43 D. D. Klug, Y. P. Handa, J. S. Tse and E. Whalley, *J. Chem. Phys.*, 1989, **90**, 2390.
44 Y. P. Handa, D. D. Klug and E. Whalley, *Can. J. Chem.*, 1988, **66**, 919.
45 G. P. Arnold, E. D. Finch, S. W. Rabideau and R. G. Wenzel, *J. Chem. Phys.*, 1968, **49**, 4365.
46 B. Minceva-Sukarova, W. F. Sherman and G. R. Wilkinson, *J. Phys. C*, 1984, **17**, 5833.
47 B. Minceva-Sukarova, G. Slark and W. F. Sherman, *J. Mol. Struct.*, 1988, **175**, 289.
48 I.-M. Chou and H. T. Haselton, *Rev. High Pressure Sci. Technol.*, 1998, **7**, 1132.
49 V. F. Petrenko and R. W. Whitworth, *Physics of Ice*, Oxford University Press, Oxford, 1999.
50 G. P. Johari, *J. Chem. Phys.*, 2003, **118**, 242.
51 C. G. Salzmann, *Relaxation und Kristallisation von hochdichtem amorphen Eis unter Druck und Charakterisierung der hergestellten Eismodifikationen IV und XII*, PhD thesis, University of Innsbruck, Innsbruck, 2003.

